RSC Publishing Faraday Discussions

FDPHOTOC15: Ultrafast Charge Transfer Dynamics in Supramolecular Pt(II) Donor-Bridge-Acceptor Assemblies: the Effect of Vibronic Coupling

Journal:	*Faraday Discussions*
Manuscript ID:	FD-ART-06-2015-000103.R1
Article Type:	Paper
Date Submitted by the Author:	25-Jun-2015
Complete List of Authors:	Scattergood, Paul; The University of Huddersfield, Chemical & Biological Sciences Delor, Milan; University of Sheffield, Department of Chemistry Sazanovich, Igor; University of Sheffield, Department of Chemistry Towrie, Michael; STFC, Central Laser Facility Weinstein, Julia; University of Sheffield, Department of Chemistry

Ultrafast Charge Transfer Dynamics in Supramolecular Pt(II) Donor-Bridge-Acceptor Assemblies: the Effect of Vibronic Coupling

Paul A. Scattergood,[1,3] Milan Delor,[1] Igor V. Sazanovich,[1,2] Michael Towrie,[2] and Julia A. Weinstein[1]*

[1] *Department of Chemistry, University of Sheffield, Brook Hill, Sheffield, S3 7HF, UK, e-mail: Julia.Weinstein@sheffield.ac.uk*
[2] *Central Laser Facility, Science and Technology Facilities Council, Harwell Science and Innovation Campus, Rutherford Appleton Laboratory, Oxfordshire, OX11 0QX, UK*
[3] *present address: Department of Chemistry, University of Huddersfield, UK*

ABSTRACT

Nuclear-electronic (vibronic) coupling is increasingly recognised as a mechanism of major importance in controlling the light-induced function of molecular systems. This paper investigates several new Donor-Bridge-Acceptor charge-transfer molecular assemblies built on a trans-Pt(II) acetylide core, which differ by the mode of attachment of the donor to the bridge. We also investigate how targeted vibrational excitation with low-energy IR light post electronic excitation can perturb vibronic coupling and affect the efficiency of electron transfer (ET) in *solution phase*. We compare and contrast properties of a range of Donor-Bridge-Acceptor Pt(II) *trans*-acetylide assemblies, where IR excitation of bridge vibrations during UV-initiated charge separation in some cases alters the yields of light-induced product states. The study discusses the molecular features necessary for external vibronic control of excited state processes, and highlights fundamental questions on the role of vibrational processes immediately following charge transfer photoexcitation in solution.

Introduction

Photoinduced electron transfer, an elementary light-induced process, is central to a wide variety of applications, particularly photocatalysis, optoelectronics and artificial photosynthesis.[1,2] Occurring on extremely fast timescales following light absorption, intramolecular photoinduced electron transfer commonly proceeds via a shift of electron density from donor to acceptor, forming a charge separated state (CSS). From this transient state, reductive and oxidative equivalents may be transferred to reactants in the generation of solar fuels, or electrons may be injected into the conduction band at a semiconductor interface.[3,4]

One strategy which may be adopted in the construction of a charge transfer assembly is the so-called 'modular approach' where several functional units are integrated within one supramolecular architecture.[5,2] These systems comprise electron-donating and -accepting groups, covalently linked together through an intermediate bridge, forming a donor-bridge-acceptor (DBA) molecular assembly. Ultrafast intramolecular electron transfer in condensed phase often competes with ultrafast intersystem crossing and vibrational relaxation.[6,7] On such timescales, the Born-Oppenheimer approximation breaks down, i.e. electronic and

nuclear degrees of freedom cannot be considered independent, and nuclear-electronic (vibronic) coupling becomes a major factor in the excited state dynamics in the multidimensional reaction landscape.[8] It is widely acknowledged that vibronic interactions between the bridge and D/A components in the DBA assemblies play a crucial role in the "choice" of a specific reaction pathway out of many available, ultimately determining product state yields.[9–1314,15] However, direct investigation of vibronic interactions in light-induced reactions is a challenging task due to the ultrafast timescales involved, the multiple vibrations coupled to charge transfer events, and coupling between vibrations of each electronic state. Therefore, how exactly vibronic coupling influences the fate of light-induced charge transfer processes is very much a question open to discussion.

A number of DBA systems centred around transition metals, particularly those featuring d^6 metal ions such as Ru(II)[16,4] and Re(I)[17,14,18–23] have proven to be highly efficacious in the production of charge separated excited states, and form an ideal test-bed for studies of ultrafast dynamics of electron transfer. Complexes of Pt(II)[24–37] are also attractive for such investigations owing to the square planar coordination environment around the metal centre, which enables control over the directionality of charge transfer via positioning of both electron donor and acceptor ligands at opposing sides of the metal centre. The utilisation of donor acetylide ligands facilitates the formation of more stable, longer-lived charge-separated states due to strong-field acetylides raising the energy of otherwise deactivating metal *dd*-states.

We have recently reported a detailed investigation[38,39] of photophysics of a Pt(II) trans-acetylide DBA system containing a naphthalimide monoimide (NAP) as an electron acceptor, and phenothiazine (PTZ) as electron donor, PTZ-CH_2-Ph-CC-Pt-CC-NAP – shown as **3-NAP** in Figure 1. This study, which combined steady-state measurements, UV-visible transient absorption spectroscopy, ultrafast time-resolved infrared (TRIR) spectroscopy, and DFT calculations, led to two important outcomes. Firstly, it revealed complex photophysics involving primary formation of a bridge-to-acceptor charge-transfer (CT) excited state, DB^+A^-, which branched over 3 different pathways – recombination of electron/hole to the ground state, recombination with formation of an acceptor-localised $\pi\pi^*$ ^{3}NAP state, and forward electron transfer forming a fully charge-separated state D^+BA^-, ie PTZ^+-NAP^-[39] (Scheme 1A). Secondly, we have demonstrated that exciting bridge vibrations in the branching CT state with an IR pulse led to a radical change in the reaction pathways, probably due to perturbation of vibronic interactions between the CT state and potential product states.[38] Specifically, one of the 3 pathways of the CT state decay in **3-NAP** has been switched off, as illustrated in Scheme 1B. These experiments require firstly collecting the data in a standard pump-probe configuration, where UV/Vis excitation pulse is followed by the probing IR pulse over a series of time delays $\{UV/Vis_{pump}\text{-}IR_{probe}\} = T$ (Scheme 1A). The same experiments are then conducted in a 3-pulse arrangement, whereby UV/Vis pump pulse is followed by an IR-pump pulse at time delays $\{IR_{pump}\text{-}UV/Vis_{pump}\} = t$; the system is then probed by a broad-band IR pulse at time delays $\{UV/Vis_{pump}\text{-}IR_{probe}\} = T$. Comparison of the transient IR spectra recorded with and without intermediate IR excitation establishes the effect of the latter on the photoinduced processes.

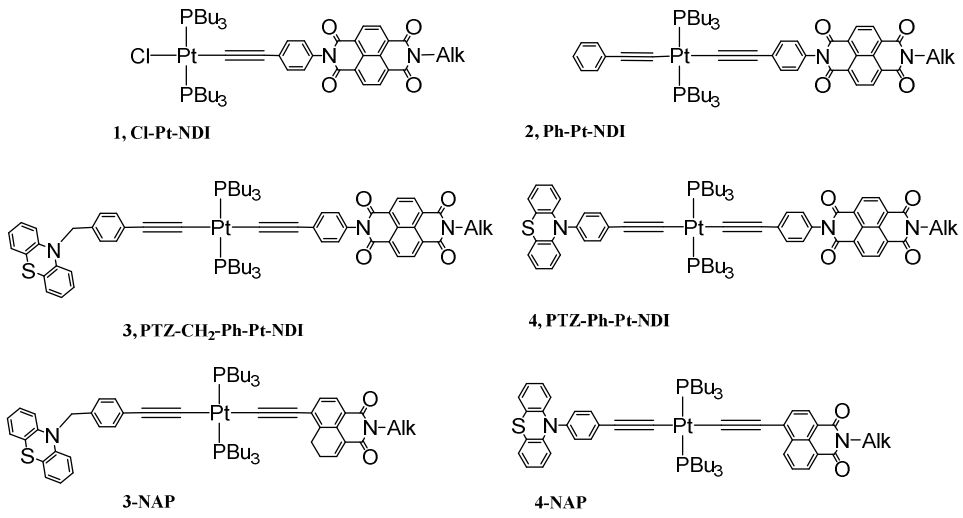

Figure 1 Structures of the Pt(II)-centred *bis*-acetylide 'Donor-Bridge-Acceptor' assemblies **3** and **4** which use naphthalene-diimide (NDI) electron acceptor investigated in this study, of the precursor compounds **1** and **2**, and of the analogous compounds **3-NAP** and **4-NAP** which use naphthalene-monoimide (NAP) as electron acceptor; Alk = $-C_8H_{17}$.

The mechanism by which this IR-control effect works is still a matter of debate. By expanding a range of DBA systems we aim to explore further how perturbing vibronic coupling in the intermediate excited state may influence the ultimate outcome of the charge transfer processes, and attempt to discuss the features necessary for such an effect to occur.

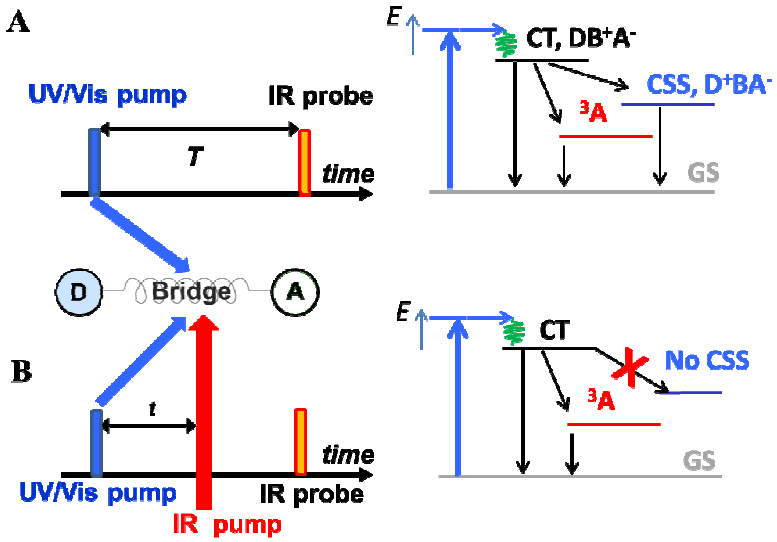

Scheme 1 Schematic description of IR-perturbation experiments, illustrated on the example of 3-NAP (Fig 1) in CH_2Cl_2, under UV/Vis pump of 400 nm, ~50 fs. (A). Pulse sequence employed in TRIR experiments (left) and energy level diagram for 3-NAP (right). (B). Pulse sequence employed in IR-control experiments, $\{UV/Vis_{pump}\text{-}IR_{pump}\text{-}IR_{probe}\}$ measurements (left) and energy level diagram (right) demonstrating the shut-down of one reaction pathway.

Here, we report on the investigation of ultrafast electron transfer in trans-acetylide Pt(II)-based DBA assemblies, and compare and contrast the light-induced behaviour of several systems featuring different electron acceptors, or different modes of attachment of the Donor and/or Acceptor. These new systems add to the growing body of *asymmetric* [Donor-C≡C-Pt-C≡C-Acceptor] motifs.[33,40–43] with electron donating and accepting ligands coordinated to the metal centre through ethynyl functionality in a *trans* arrangement.

All complexes feature a powerful donor, phenothiazine (PTZ), combined with a naphthalene-diimide (NDI) as an electron acceptor. Aromatic acid imide acceptor groups[44–47] have been used in diverse charge-transfer assemblies[30,31,48,49] owing to their low reduction potentials, and the ability to form stable radical-anions which possess distinct and intense absorptions in both UV-Vis and IR spectral ranges.[46,49,50] Of direct relevance to this work, NDI has previously featured as an electron trap in oligomeric Pt(II) systems designed to study charge mobility.[36,42,51] The presence of strong IR reporters (ν(C=O) and ν(C≡C)) along the DBA assemblies enables the use of time-resolved infrared spectroscopy as the most suitable means to investigate vibrational/vibronic coupling in the course of charge transfer.

The lowest excited state in the previously studied system **3-NAP** was the acceptor localised triplet state, ^{3}NAP. Changing the electron acceptor from NAP to NDI considerably decreases the reduction potential of the acceptor and therefore the energy of the charge-separated state, whereas the NDI triplet state is higher in energy (2.1 eV vs. 1.9 eV for ^{3}NAP),[50] thus the lowest excited state in "PTZ-Pt-NDI" assemblies is expected to be a charge-separated state.

To enable a step-wise charge-transfer process, the donor moiety in PTZ-CH_2-Ph-Pt-NDI (**3**) is connected to the Pt-acetylide bridge through a saturated linker, being effectively "decoupled" from the bridge. The excited state dynamics of this system is compared to PTZ-Ph-Pt-NDI (**4**), where the PTZ donor is directly attached to the bridge. Intriguingly, such subtle modification of the supramolecular architecture results in a dramatic change in photoinduced dynamics, and alters the lifetime of the resulting charge-separated state by nearly an order of magnitude. The attempted three-pulse {UV/Vis pump – IR pump – IR-probe} experiments aimed at altering the reaction pathways by IR excitation of bridge vibrations in the intermediate excited state are also described, and compared/contrasted to those for the corresponding NAP-based assemblies **3-NAP** and **4-NAP**.

Results and Discussion

Synthesis

Acceptor ligand **L1**, *N*-octyl-*N*'-(*p*-ethynylphenyl)-1,4,5,8-naphthalene tetracarboxylic diimide,[42,51] and the ethynyl tolyl-*N*-phenothiazine ligand L3[25]were prepared as described previously. The ethynylphenyl-*N*-phenothiazine ligand **L2** was prepared via a 5-step procedure, making use of a previously reported Pd(0)-catalysed N-C coupling methodology[52] to append phenothiazine with a phenyl ring. Briefly (Scheme 2), commercially available 1,4-dibromobenzene was converted to 1-bromo-4-trimethylsilyl-benzene through lithiation and

subsequent quenching with trimethylsilylchloride. This was followed by Pd(0)-catalysed cross-coupling with phenothiazine in the presence of ^{t}BuOK and P^{t}Bu$_3$, proceeding with a good yield of 82%. Iodination of the trimethylsilyl group with iodine monochloride thus permitted the further Sonogashira cross-coupling with trimethylsilylacetylene, with later removal of the TMS protecting group with K_2CO_3 in MeOH furnishing the final ethynyl-terminated ligand.

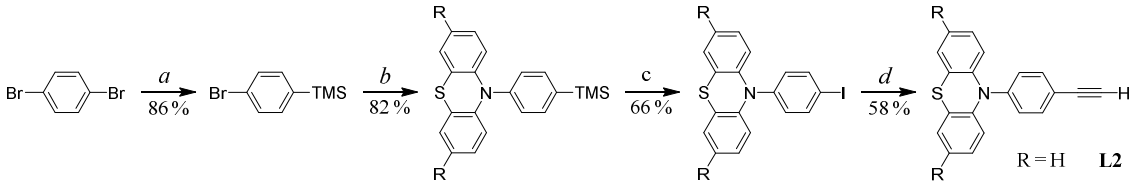

Scheme 2 (a): i) *n*-BuLi, Et_2O, -78 ^{o}C, 1.5h. ii) TMS-Cl, 25 ^{o}C, 1.5h. (b): Phenothiazine, Pd(dba)$_2$, ^{t}BuOK, P^{t}Bu$_3$, toluene, 60 ^{o}C, 3 days. (c): ICl, MeCN / CH_2Cl_2, 0-25 ^{o}C, 24h. (d): i) Trimethylsilylacetylene, Pd(PPh$_3$)$_2$Cl$_2$, CuI, Et_3N, benzene, r.t., 3.5 days. ii) K_2CO_3, THF/MeOH, r.t. 18h.

Linear, *trans* 'acceptor-Pt-donor' *bis*-acetylide complexes (figure 1) were constructed *via* a stepwise procedure, making use of the previously reported 'acceptor-Pt' dyad synthon **1**. Formation of this mono-acetylide complex itself utilises copper-free reaction conditions, proceeding from *cis*-Pt(PBu$_3$)$_2$Cl$_2$ and the appropriate ethynyl ligand (**L1**) in a refluxing amine solution. Whilst **1** has been widely and effectively employed in the iterative-convergent synthesis of short chain Pt(II) oligomers,[42] it is applied here as a precursor to asymmetric mono-nuclear Pt(II) complexes **2-4**. Subsequent Hagihara coupling of **1** with ethynyl functionalised electron donor ligands affords triadic 'acceptor-Pt-donor' systems in moderate yields of typically 65-75 %. Each of the bis-acetylide complexes **2-4** was confirmed to be formed with exclusively *trans* configuration at the metal centre by ^{31}P NMR spectroscopy, with the magnitude of the diagnostic ^{195}Pt-^{31}P coupling interaction being of the order of 2300 Hz ($J_{Pt\text{-}P}$ for a *cis bis*-phosphine configuration is typically 3500 Hz). It is noted that the employment of this stepwise procedure affords a greater degree of overall synthetic control; permitting the use of a wide variety of ethynyl ligands, avoiding the production of statistical mixtures of Pt(II) *bis*-acetylide complexes and with the isolation and characterisation of a Pt(II) dyad greatly assisting in the structural and photophysical study of the much larger triadic assemblies.

UV-Visible Electronic Absorption Spectroscopy and electrochemistry

UV-Visible electronic absorption spectra for CH_2Cl_2 solutions of **1-4** (figure 2) are dominated by three intense bands centred at 380, 360 and 340 nm, attributed to intra-ligand π-π* transitions localised on the naphthalene diimide (NDI) fragment, with the characteristic vibronic progression of the S_0-S_1 electronic transition.[50,51,53–55]

A range of additional, overlapping, higher energy transitions observed for **2-4**, especially two prominent features centred at 327 and 341 nm but not in **1** allows their assignment to intra-

ligand transitions associated with the Pt(II)-centred *bis*-acetylide bridging unit. An additional absorption band at >400 nm, with the extinction coefficient of an order of 100 dm^3 $mol^{-1}cm^{-1}$ observed in **2**-**4** implies a presence of a charge-transfer transition.

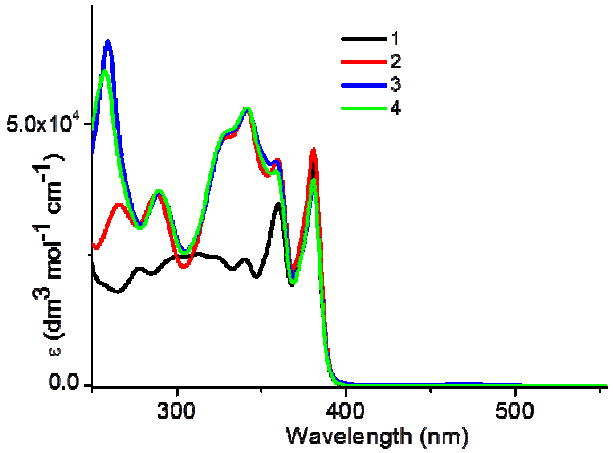

Figure 2 Ground state electronic absorption spectra for CH_2Cl_2 solutions of Pt(II) complexes **1**-**4**, recorded at room temperature.

Reduction: Complexes **1**-**4** display two, well separated, reversible reduction processes in the region of -1.05 and -1.45 V. Both of these processes are assigned to the sequential reduction of the NDI moiety. The reduction potentials measured here are in very good agreement with those reported previously for NDI-containing systems, where it is also confirmed that each reduction process is one-electron in nature.[56,57] The electrochemical data displayed in table 1 clearly show that there is no variation in NDI reduction potential as the substituent positioned *trans* at the metal centre is altered. This suggests that the NDI fragment is electrochemically decoupled from the *bridge*, likely due to their mutually orthogonal arrangement.[50] As both reduction processes are NDI-based, it is concluded that the lowest unoccupied molecular orbital (LUMO), and the LUMO+1, are localised predominantly on the NDI ligand.

Oxidation: The Pt(II) mono-acetylide precursor **1** displays one irreversible oxidation at +1.03 V. The shape and anodic peak potential of this process is characteristic of Pt(II) acetylides,[25,57,58] being attributed to the removal of electrons from a molecular orbital based upon the metal centre and coordinated ethynyl group. A similar oxidation is observed for the *bis*-acetylide model complex **2** at +0.80 V, with the cathodic shift being due to substitution of the electron withdrawing chloride for a phenylacetylene ligand. In this instance, oxidation is predicted to involve a more diffuse molecular orbital comprising of contributions from both complexed ethynyl groups in addition to the metal centre. Consequently, for **1** and **2** the highest occupied molecular orbital (HOMO) is determined to be localised predominantly across the Pt(II)-centred bridging unit. *Bis*-acetylide complexes featuring a phenothiazine donor (**3, 4**) display one electrochemically reversible oxidation within the potential window shown in figure 3, at +0.33 and +0.25V, resp. This process is attributed to an oxidation

localised on the phenothiazine entity itself. Complexes **3** and **4** also have additional oxidation processes occurring above +0.8 V (table 1), which could not be assigned with confidence owing to the processes not being fully electrochemically reversible. Direct incorporation of the PTZ in the Ph-acetylide moiety in **4** vs. **3** leads only to a small, ca. -0.08 V shift in the oxidation potential.

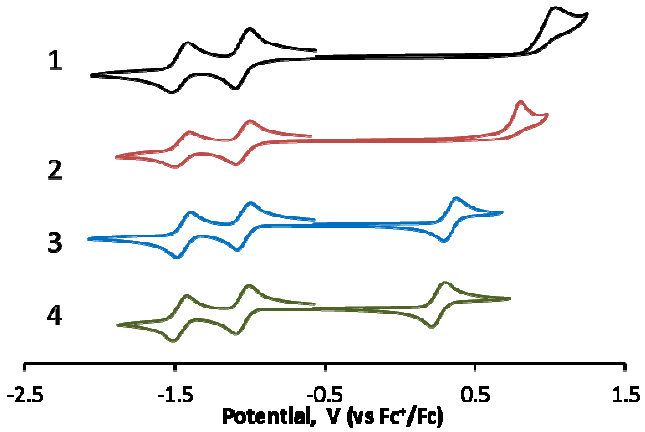

Figure 3 Cyclic voltammograms for 1.5 mM CH_2Cl_2 solutions of **1-4**. Scans shown were recorded at 100 mVs^{-1} at room temperature with 0.2 M $[^nBu_4N][PF_6]$ as supporting electrolyte. Potentials are reported against the Fc/Fc^+ reference.

Table 1 Electrochemical data of **1-4** recorded in CH_2Cl_2 at r.t. Scan rate 100 mVs^{-1}. All potentials are quoted in V vs the Fc/Fc^+ couple. Anodic-cathodic peak separations $\Delta E_{a,c}$ are shown in mV within brackets where applicable, $\Delta E_{a,c}$ for Fc/Fc^+ was typically 90 mV.

	Reduction, V	**Oxidation, V**
1, Cl-Pt-NDI	-1.46 (105), -1.05 (104)	+1.03[a]
2, Ph-Pt-NDI	-1.45 (99), -1.05 (95)	+0.80[a]
3, PTZ-CH_2-Ph-Pt-NDI	-1.44 (90), -1.04 (88)	+0.33 (86), +0.85[b]
4, PTZ-Ph-Pt-NDI	-1.47(91), -1.05 (90)	+0.25 (87), +0.97

[a] electrochemically irreversible under experimental conditions used. [b] Quasi-reversible.

It is expected that the lowest excited state in **3** and **4** will be the charge-separated state, since its energy estimated from electrochemical data as ~1.8 eV, lies below that of the ^{3}NDI (ca. 2.1 eV).[50] The Pt-acetylide bridge is decoupled from the acceptor as the latter is orthogonal to the intermediate phenyl ring, and no strong MLCT band is observed in visible region (Fig 2). We therefore use 380 nm, ~50 fs excitation pulse to populate the ^{1}NDI* singlet excited state to trigger subsequent charge transfer.

Photoinduced charge separation in DBA assemblies

The dynamics of **3** and **4** was studied using ultrafast TRIR, picosecond electronic transient absorption spectroscopy, and nanosecond flash photolysis (data shown in the SI).

The FTIR spectrum for PTZ-CH_2-Ph-Pt-NDI is shown in Figure 4. The major features of interest are the NDI-localised ν(C=O) symmetric/asymmetric combinations forming the four bands at 1669 cm^{-1}, 1680 cm^{-1}, 1708 cm^{-1} and 1718 cm^{-1}, as well as the bridge-localised ν(C≡C) asymmetric combination at 2101 cm^{-1} with a weak shoulder around 2115 cm^{-1} due to the symmetric combination. There are many weaker transitions in the 1480-1640 cm^{-1} range due to phenyl, PTZ and NDI ring modes. The assignment of NDI-based vibrations in the neutral and anionic forms of NDI obtained by IR spectroelectrochemistry of Pt(phen-NDI)Cl_2 was reported elsewhere:[50] the ν(C=O) of the NDI were shown to shift to substantially lower energies with characteristic positions at 1514 cm^{-1}, 1592 cm^{-1}, 1631 cm^{-1}, and 1660 cm^{-1} upon one-electron reduction.

Excitation with a ~50 fs, 380 nm pulse results in an instantaneous bleaching of the ground state IR absorption bands, and formation of several transient bands which evolve in time. The TRIR spectra of PTZ-CH_2-Ph-Pt-NDI, **3** at several time delays following excitation, and decay associated spectra (DAS) obtained from global analysis of the data (using a sequential model with four kinetic components, A→B→C→D→E, where A is the state initially populated by laser excitation and E is the ground state) are shown in Figure 5. 380 nm excitation instantaneously populates an NDI-localised singlet excited state (^{1}NDI*). Subsequently bands at 1514, 1589 and 1630 cm^{-1}, which correspond to the aforementioned ν(C=O) combination bands in the reduced NDI form, grow in with τ_1 = 1 ± 0.1 ps. This spectral evolution evidences electron transfer to NDI within 1 ps of laser excitation.

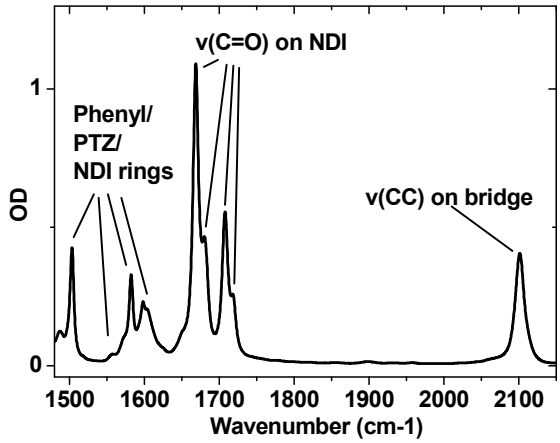

Figure 4 FTIR spectrum for PTZ-CH_2-Ph-Pt-NDI (**3**) in CH_2Cl_2 in the region probed by TRIR. Note that the spectra of the two other NDI trans-acetylide complexes show very similar features and are not shown for clarity.

Bands at 1567 and 1895 cm^{-1} also grow in with τ_1 = 1 ps. The 1895 cm^{-1} band is assigned to ν(C≡C) when the Ph-C≡C-Pt-C≡C bridge is oxidised: the decrease in the IR frequency is

consistent with a decrease of electron density on the bonding orbital, weakening the C≡C bond; and also with partial delocalisation across the brdige, which somewhat reduces the bond order. The position and profile of the 1895 cm^{-1} band also closely resemble bridge-to-acceptor charge transfer in NAP-containing systems, indicating a similar electron density environment experienced by the bridge.[39] We thus assign this signal to a bridge-to-NDI charge transfer (CT), where electron density is shifted from the Ph-C≡C-Pt-C≡C bridge to the NDI acceptor.

The 1895 cm^{-1} CT band decays with two time constants: τ_2 = 6.0 ± 0.5 ps, reflecting a narrowing and slight blue-shift of the band (DAS2, see difference between 1 ps spectrum and 10 ps spectrum on **Figure 5**A), and τ_3 = 40 ± 2 ps for a full decay (DAS3). A band at 1567 cm^{-1} follows exactly the same kinetic evolution, suggesting it is also a bridge-localised mode; this is tentatively assigned as a phenyl ring mode. We note that a sequential model does not take into account a minor contribution of ground state recovery which also occurs during the 6 and 40 ps processes, indicating some branching in the CT excited state.

The 40 ps decay gives rise to a band at 2095 cm^{-1}, partially overlapped with the ν(C≡C) ground state bleach. This closely resembles the ν(C≡C) band in the CSS of the analogous complex PTZ-CH_2-Ph-Pt-NAP,[39] as well as in the diimine Pt(II) acetylide cascade, (PTZ-CH_2-Ph-CC-)$_2$Pt(phen-NDI).[59] The presence of this band indicates that the partially oxidised bridge was quenched by electron transfer from the PTZ donor on a 40 ps timescale, forming the full CSS, [PTZ^+NDI^-]. No spectral evolution was observed after ~200 ps up to the ~3 ns time limit of the TRIR experiment. Flash photolysis measurements provide a lifetime of 130 ± 10 ns (SI) for the charge-separated state. Kinetic traces at selected frequencies obtained from TRIR data for **3** (Fig 5), fitted using a sequential model with four exponential functions, are shown in Fig. 6A.

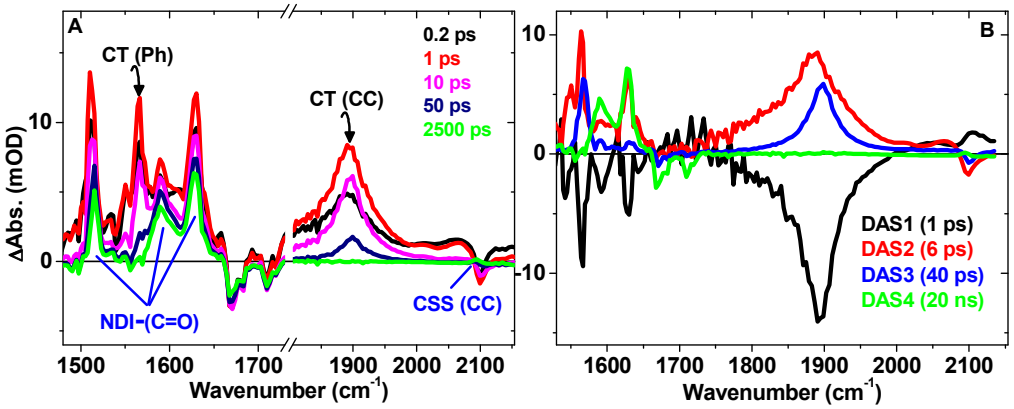

Figure 5 TRIR spectra at representative delay times (A) and DAS extracted from global analysis of the TRIR data using a sequential model with 4 exponential functions (B) for PTZ-CH_2-Ph-Pt-NDI in CH_2Cl_2. The extracted lifetimes are τ_1 = 1 ± 0.1 ps, τ_2 = 6.0 ± 0.5 ps, τ_3 = 40 ± 2 ps, τ_4 = 20 ± 10 ns (a constant on the time scale studied in TRIR). The last parameter is not reliable as the signal barely decays on the maximum timescale of the experimental setup since the lifetime of the final excited state determined by flash photolysis, is 130 ns.

Overall, the excited state processes in PTZ-CH_2-Ph-Pt-NDI can be described by the sequence of events illustrated in Fig 8, C. The excited states considered are singlet ligand-centred state ^{1}NDI* (denoted as orange bar in Fig 8), a charge transfer state **CT** formed as a result of electron transfer from the bridge to the NDI (black bar, Fig 8), and the full charge-separated state **CSS** (blue bar, Fig. 8). 380 nm excitation populates the singlet ligand-centred state ^{1}NDI*.[50] This process initiates electron transfer from the bridge to NDI on a 1 ps timescale, forming a CT state, [PTZ-B$^+$-NDI$^-$]. Here we assume singlet-to-triplet intersystem crossing has already occurred within this 1 ps process due to the direct involvement of Pt orbitals in the first electron transfer step. Following this initial rapid electron transfer, several processes are expected to occur, including intramolecular structural reorganisation to favour bridge-to-NDI conjugation, solvent reorganisation following dipole and structural change, and vibrational energy redistribution. These processes are convolved in the 6-ps component. The CT state has a 40 ps lifetime, dictated by the rate of reductive quenching of the oxidised bridge by electron transfer from the PTZ donor, resulting in the CSS [PTZ$^+$NDI$^-$]. This final excited state has a 130 ns lifetime.

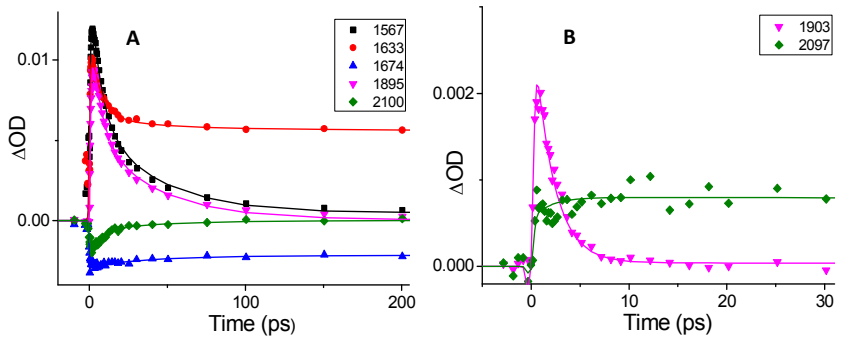

Figure 6 Kinetic traces obtained from TRIR data at selected frequencies shown. (A) For PTZ-CH_2-Ph-Pt-NDI (**3**), using the data in Fig. 5. Symbols – experimental data, solid lines – results of the fit in a sequential model with four exponential functions. (B) For PTZ-Ph-Pt-NDI (**4**), using the data shown in Fig. 7. Symbols – experimental data, solid lines – results of the fit in a sequential model with two exponential functions. See text for the values of the lifetimes.

Removal of a -CH_2- spacer between the Donor and the Bridge in **4** vs. **3** leads to dramatic changes in photoinduced processes, illustrated schematically in Fig 8D. The TRIR spectra for **4**, along with the DAS obtained through global analysis using a 2-component sequential kinetic model (A→B→C), are presented in Figure 7. The TRIR spectra for **4**, PTZ-Ph-Pt-NDI show spectral signatures identical to that of **3**, but strikingly different kinetic behaviour. Transient bands at 1514, 1589 and 1630 cm^{-1} associated with ν(C=O) combination bands in the reduced NDI form grow in within the ~200-fs instrument response time following 380 nm excitation. The C≡C and phenyl modes at 1907 cm^{-1} and 1567 cm^{-1} associated with the CT state are also present immediately after excitation, and decay monoexponentially with lifetime τ_1 = 2.0 ± 0.1 ps, forming the full CSS (characteristic absorption at 2097 cm^{-1}

partially overlapping with the ground state). The latter, final, state fully decays with a 3 ns lifetime to the ground state, contrasting with the 130 ns CSS lifetime determined in **3**.

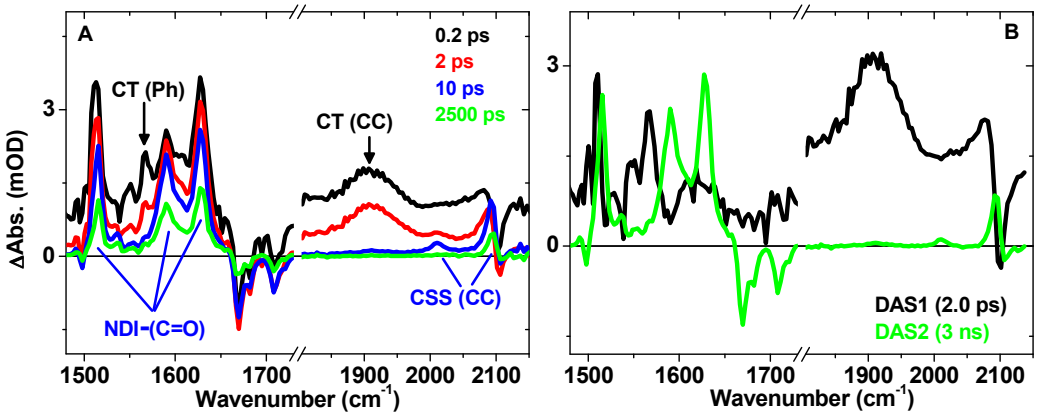

Figure 7 TRIR spectra at representative delay times (A) and DAS extracted from global analysis of the TRIR data using a sequential model with 2 exponential functions (B) for PTZ—Ph-Pt-NDI, **4**, in CH_2Cl_2. The extracted lifetimes are $\tau_1 = 2 \pm 0.1$ ps, $\tau_2 = 3 \pm 1$ ns.

This kinetic behaviour in **4** is surprising. The only difference between **3** and **4** is in the attachment of the donor: the removal of the saturated linker extends conjugation of the acetylide bridge towards the donor moiety (*cf* a small shift on oxidation potentials, *vide supra*); there is no change in ground state reduction potential, or absorption maximum. It is thus unexpected that the initial bridge-to-acceptor charge transfer following excitation into ^{1}NDI* is significantly affected. However, the lack of grow-in at early times indicates otherwise, suggesting a rate of charge transfer being at least 5 times larger in PTZ-Ph-Pt-NDI. Reductive quenching of the oxidised bridge by the donor then proceeds in 2 ps in **4** compared to 40 ps in **3**, and similarly charge recombination occurs with a lifetime of 3 ns in **4** vs. 130 ns in **3**. Further, lack of evidence of ground state recovery prior to the formation of the CSS in PTZ-Ph-Pt-NDI indicates that the bridge-to-acceptor CT state converts fully into the CSS without any other branching pathway, in contrast to PTZ-CH_2-Ph-Pt-NDI.

The reduction of the CT lifetime from 40 ps to 2 ps and CSS lifetime from 130 ns to 3 ns could be caused by the higher degree of conjugation of the donor ligand into the bridge. Furthermore, an increase in conjugation on the donor side may have an inductive effect on the bridge-to-NDI CT driving force, resulting in an increased rate of electron transfer to NDI in the primary step. In the analogous NAP-containing complexes, removal of the CH_2 spacer increases the rates of charge separation and recombination by a factor of 5, i.e. to a much lesser extent than in NDI-containing complexes. This discrepancy is not fully understood at the moment but is presumed to be due to a number of effects which includes: different energetics between NAP- and NDI-containing complexes, altered bridge geometries which modify bridge-to-acceptor coupling significantly (note the additional phenyl ring between Pt-C≡C and the acceptor in NDI complexes compared to NAP complexes), and a difference in branching pathways whereby NAP-containing complexes consistently have an additional (and dominant) channel to the intraligand ^{3}NAP state.

One of the goals of the current study was to develop further insights into the mechanism of the "IR-control" effect discussed in the introduction, whereby perturbing an intermediate excited state (e.g., a CT state here) by an IR pulse can affect excited state pathways. Experiments attempting IR-control of electron transfer processes in **3** and **4** have been undertaken following the methodology described previously.[38,60] Briefly, we used an ultrafast UV(pump)-IR(pump)-IR(probe) pulse sequence, in which an intermediate narrow-band (~12 cm^{-1}, ~1.5 ps) IR-pump is introduced at different time delays, from the instrument-limited ~2 ps to the time delay of approximately three-fold that of the lifetime of the intermediate CT state. The effect was probed by broadband IR pulses as in TRIR experiments, and the differential signals of TRIR{IRpumpON-IRpumpOFF} were analysed – should IR-pump had an effect, such a differential signal would be present. However, no effect on the excited state processes in **3** and **4** was observed neither upon IR-excitation of ν(C≡C), nor of the other prominent IR-bands of the CT excited state under a variety of experimental conditions. This lack of effect is in stark contrast with the analogous **3-NAP** and **4-NAP** compounds.

A comparison between different systems which do or do not exhibit an IR-control effect under our experimental conditions is presented in table 2 and in Figure 8. It is clear that the requirements for the IR-control to take place include: (i) a gateway state, e.g., a CT state, which branches over several pathways; (ii) that this branching should occur on timescales comparable to vibrational relaxation along the electron transfer reaction coordinate (i.e. the 40-ps lifetime of the CT state in **3** is too long); (iii) that the difference in energy between the gateway state and the nearest lower excited state should be of the order of vibrational energies, up to 0.3 – 0.4 eV (i.e. the 0.6 eV difference in **4** may be too large).

However, fulfilling these conditions does not necessarily allow for IR-control to take place. Other factors, for example the mode of coupling between the acceptor and the bridge – which is very different between **3** and **3-NAP** – may also play an important role, and highlights the question on the mechanism of vibronic coupling in such systems.

Table 2. Comparison of excited state parameters related to the possibility to influence excited state behaviour by IR-pump of the intermediate excited state. See Fig. 8 for details.

Compound	**3-NAP**[a]	**4-NAP**[c]	**3**	**4**
τ(CT), ps	14	2	40	3
ΔG CT – CSS, eV[b]	0.2	0.4	0.5	0.6
CT branching	Yes	Yes	Minor	No
Effect of IR-pump of ν(CC) in the CT state?	Yes	Yes	No	No

[a] From ref.[38,61]; [b] estimated from emission data where available, and electrochemical data; [c] from ref[60] .

Conclusion

New Donor-Bridge-Acceptor triads based on trans-Pt(II) acetylide bridge have been prepared and fully characterised, with the aim to investigate the possibilities of perturbation of reaction pathways by affecting specific vibrations coupled to charge separation and recombination. Such *trans*-acetylide systems offer opportunities for tuning the distance, the coupling between the components, and the relative energetics of the excited states of different orbital nature through careful engineering of the ligands. The subtle change in the mode of attachment of the D unit to the bridge (with or without an intervening CH_2 saturated linker) modifies the energy of the CSS by a marginal 0.08 eV, but induces a dramatic, nearly order of magnitude change in the dynamics, accelerating both charge separation and charge recombination.

Comparing the systems which do and do not exhibit vibrational control of electron transfer suggests some features necessary for such an effect to occur. These conditions relate to the lifetime of the transient state, energetic difference between the states involved, and the character of electronic/vibronic coupling along the assembly. Furthermore, structural reorganisation of the bridge and the accompanying vibrational relaxation seem to considerably affect electron transfer rates and propensity. It is thus expected that bridge-localised vibronic interactions play a crucial role in determining photochemical pathways in such supramolecular systems. Detailed investigations of the effect of different factors listed above on the efficiency of "IR-control" may hopefully create a general basis of designing DBA assemblies in which reactivity can be directed by IR-light.

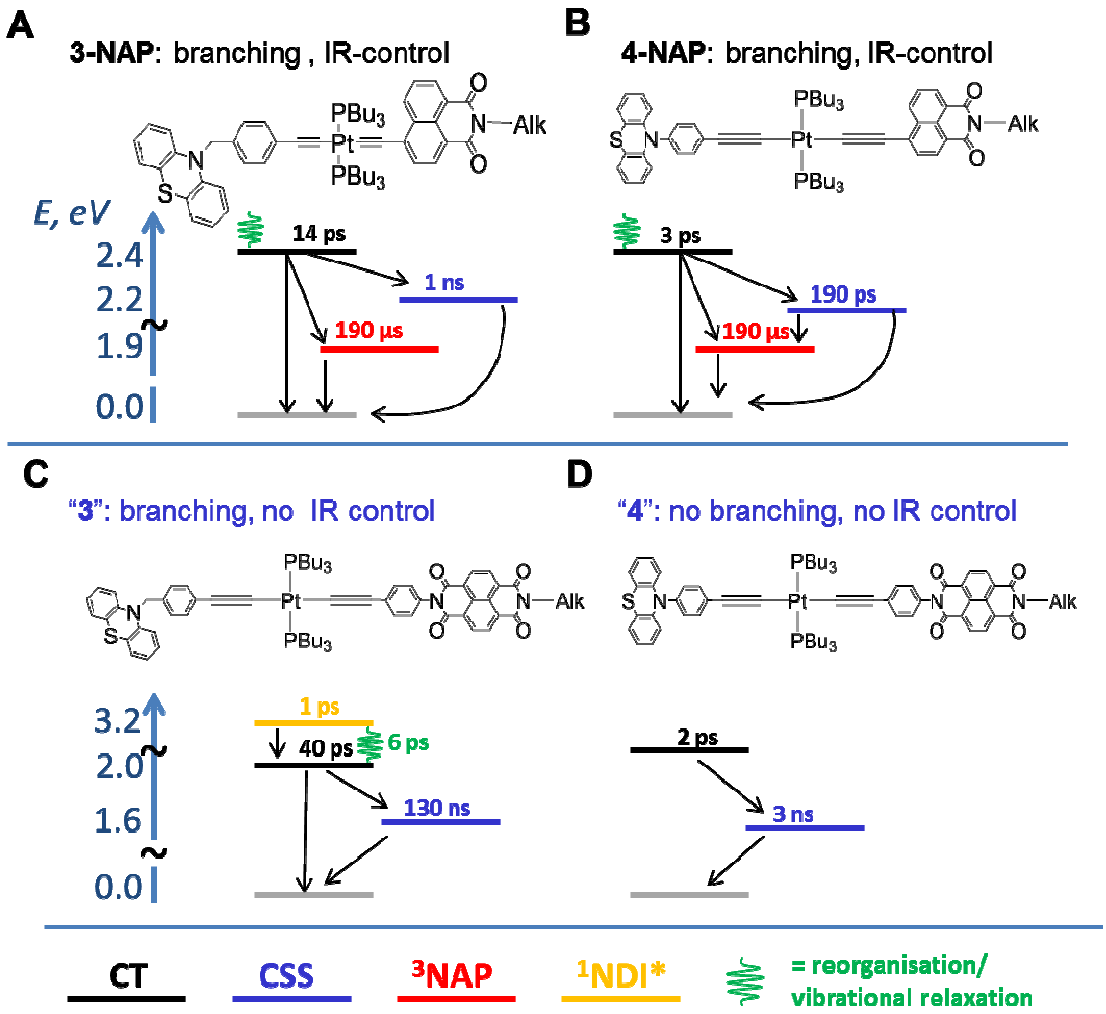

Figure 8. A summary of excited state dynamics and relative energy levels of the DBA systems build on naphthalene-diimide, labelled **3 and 4**, and the corresponding DBA systems with a weaker electron acceptor, naphthalene-monoimide, labelled as **3-NAP and 4-NAP**. Excited state are color-codes as follows: singlet acceptor-centred excited state, ^{1}NDI* - orange; triplet acceptor-centered excited state, ^{3}NAP – green; charge-transfer excited state $DB^{+}A^{-}$ (CT) - black; and full charge-separated state $D^{+}BA^{-}$ (CSS) - blue.

Acknowledgements

We are grateful for the support of the Engineering and Physical Sciences Research Council (EPSRC), the University of Sheffield, and the Science and Technology Facilities Council (STFC). We would like to thank Prof. Anthony W. Parker and Dr Greg Greetham (STFC), and Dr A J H M Meijer (University of Sheffield) for collaboration and discussions.

Experimental

General Methods

All reagent grade solvents and chemicals were used as received without further purification unless otherwise stated. All synthetic manipulations were carried out under an atmosphere of Ar, employing standard Schlenk line techniques. 'Deaeartion' of solvents was performed through vigorous bubbling with Ar for a period of at least 15 minutes. All dry solvents were obtained from a Grubbs solvent purification column.

Instrumentation

^{1}H and ^{31}P NMR spectra were collected on Bruker Avance 400, Bruker DPX-400 and Bruker Avance 250 spectrometers. Deuterated solvents of spectroscopic grade were purchased from Sigma-Aldrich. All chemical shifts are quoted in ppm, with ^{1}H NMR spectra calibrated relative to the residual solvent signal ($CDCl_3$: 7.26, d_6-Acetone: 2.05, CD_2Cl_2: 5.32).

UV-Visible absorption spectra were recorded on a Cary 50 Bio spectrophotometer, utilising quartz cuvettes of 1cm pathlength. Cyclic voltammograms were measured using an Autolab Potentiostat 100 with General Purpose Electrochemical Software (GPES). Analyte solutions were prepared using dry dichloromethane obtained from a Grubbs solvent purification column. Measurements were conducted at room temperature under a stream of dry nitrogen at scan rates varying between 20-500 mVs^{-1}. [$^{n}Bu_4N$][PF_6] was used as a supporting electrolyte, being recrystallised from ethanol and oven dried prior to use, with a typical solution concentration of 0.2 M. The working electrode was a glassy carbon disc. Pt wire was utilised as the counter electrode. The reference electrode was Ag/AgCl, being chemically isolated from the analyte solution by an electrolyte containing bridge tube tipped with a porous frit. Ferrocene was employed as an internal reference, with all potentials quoted relative to the Fc/Fc^{+} couple.

Nanosecond Flash Photolysis studies were conducted on a home-built setup based on a tuneable Ti:Sapph laser, time resolution ca. 25 ns. Picosecond TRIR studies were performed in the Ultrafast Spectroscopy Laboratory, Rutherford Appleton Laboratory, UK, ULTRA facility.[62] Briefly, double pump experiments use optical choppers modulating the repetition rate of the UV pump at 5 kHz and IR pump at 2.5 kHz while the probe pulse is at 10 kHz, facilitating the simultaneous collection of background, {UV/Vis_{pump} IR_{probe}} (TRIR); {IR_{pump} IR_{probe}}; and {UV/Vis_{pump} IR_{pump} IR_{probe}} spectra. The UV pump pulsewidth was the second harmonic of an 800 nm, 50 fs, 300 cm^{-1} pulsewidth titanium sapphire laser; the IR pump pulsewidth was 1.5 ps, ~12 cm^{-1}; the IR probe pulsewidth was ca. 100 fs, ~350-400 cm^{-1}, depending on the detection region. Analysis of ultrafast time-resolved data was performed using the open-source software Glotaran v1.3.[63]

Synthesis

Synthesis of Cl-Pt-NDI (1) is given in the SI.

Ph-Pt-NDI (2): 1 (70 mg, 0.063 mmol), phenylacetylene (20 μl, ρ = 0.93 g/ml, 0.182 mmol) and CuI (5 mg, 0.026 mmol) were dissolved in deaerated $^{i}Pr_2NH$ (12 ml) and stirred at 35 ^{o}C in the dark for 3 days. The solution was cooled to room temperature and the solvent removed to yield a bright orange coloured residue. Purification was achieved by column chromatography (Al_2O_3, gradient elution, 1:4 CH_2Cl_2 / hexane to 1:1 CH_2Cl_2 / hexane), affording the bright red-orange coloured product. Yield 33 mg, 44 %. ^{1}H NMR (d_6-Acetone, 400 MHz): 0.88 (t, *J* = 7.04 Hz, 3H), 0.95 (t, *J* = 7.32 Hz, 18H), 1.25-1.57 (m, 22H), 1.65-1.79 (m, 14H), 2.16-2.31 (m, 12H), 4.16 (t, *J* = 7.56 Hz, 2H), 7.10 (tt, *J* = 1.48, 7.12 Hz, 1H), 7.18-7.28 (m, 4H), 7.30 (d, *J* = 8.52 Hz, 2H), 7.41 (d, *J* = 8.44 Hz, 2H), 8.74-8.80 (m, 4H). ^{31}P NMR (d_6-Acetone, 101 MHz): 3.82 (J_{Pt-P} = 2367 Hz). MALDI-MS: m/z = 1178.5 (M^+).

PTZ-CH_2-Ph-Pt-NDI (3):

1 (149 mg, 0.134 mmol), *N*-(4-ethynylbenzyl)-phenothiazine (**L3**) (89 mg, 0.284 mmol) and CuI (20 mg, 0.105 mmol) were dissolved in degassed $^{i}Pr_2NH$ (20 ml) and stirred at 40 ^{o}C in the dark for 45 hours. The solvent was removed and the residue purified via column chromatography (Al_2O_3, gradient elution, 1:4 DCM / hexane to 1:1 DCM / hexane) to give the pale brown coloured product. Yield 45 mg, 24 %. ^{1}H NMR ($CDCl_3$, 400 MHz): 0.85-0.96 (m, 21H), 1.23-1.50 (m, 22H), 1.56-1.66 (m, 12H), 1.71-1.81 (m, 2H), 2.06-2.21 (m, 12H), 4.21 (t, *J* = 7.68 Hz, 2H), 5.02 (s, 2H), 6.64 (dd, *J* = 0.88, 8.16 Hz, 2H), 6.85 (td, *J* = 1.04, 7.52 Hz, 2H), 6.96 (td, *J* = 1.56, 7.76 Hz, 2H), 7.07 (dd, *J* = 1.56, 7.60 Hz, 2H), 7.10-7.16 (m, 4H), 7.23 (d, *J* = 8.24 Hz, 2H), 7.41 (d, *J* = 8.48 Hz, 2H), 8.79 (s, 4H). ^{31}P NMR ($CDCl_3$, 400 MHz): 3.16 (J_{Pt-P} = 2350 Hz). MALDI-MS: m/z = 1190.6 (M^+-PTZ).

PTZ-Ph-Pt-NDI (4): 1 (109 mg, 0.098 mmol), *N*-(*4*-ethynylphenyl)-phenothiazine (**L2**) (73 mg, 0.24 mmol) and CuI (4 mg, 0.02 mmol) were dissolved in deaerated $^{i}Pr_2NH$ (20 ml) and stirred at 35 ^{o}C in the dark for 2 days. The solvent was removed and the crude residue purified by column chromatography (Al_2O_3, gradient elution, 1:4 to 1:1 CH_2Cl_2 / hexane), with the pale yellow coloured fraction being collected and evaporated to dryness to afford the dark green product. Yield 78 mg, 58 %. ^{1}H NMR (d_6-Acetone, 400 MHz): 0.88 (t, *J* = 6.96 Hz, 3H), 0.97 (t, *J* = 7.32 Hz, 18 H), 1.24-1.60 (m, 22H), 1.68-1.81 (m, 14H), 2.20-2.34 (m, 12H), 4.17 (t, *J* = 7.56 Hz, 2H), 6.27 (dd, *J* = 1.12, 8.20 Hz, 2H), 6.84 (td, *J* = 1.20, 7.44 Hz, 2H), 6.92 (td, *J* = 1.68, 7.52 Hz, 2H), 7.06 (dd, *J* = 1.56, 7.52 Hz, 2H), 7.25-7.34 (m, 4H), 7.42 (d, *J* = 8.44 Hz, 2H), 7.53 (d, *J* = 8.40 Hz, 2H), 8.74-8.80 (m, 4H). ^{31}P NMR (d_6-Acetone, 162 MHz): 3.91 (J_{Pt-P} = 2358 Hz). MALDI-MS: m/z = 1375.3 (M^+).

REFERENCES

1 V. Balzani, *Electron Transfer in Chemistry*, Wiley-VCH, Weinheim, 2001.

2 J. J. Concepcion, R. L. House, J. M. Papanikolas and T. J. Meyer, *Proc. Natl. Acad. Sci. U. S. A.*, 2012, **109**, 15560–15564.

3 V. Balzani, G. Bergamini, F. Marchioni and P. Ceroni, *Coord. Chem. Rev.*, 2006, **250**, 1254–1266.

4 S. Karlsson, J. Boixel, Y. Pellegrin, E. Blart, H.-C. Becker, F. Odobel and L. Hammarström, *J. Am. Chem. Soc.*, 2010, **132**, 17977–17979.

5 J. H. Alstrum-Acevedo, M. K. Brennaman and T. J. Meyer, *Inorg. Chem.*, 2005, **44**, 6802–6827.

6 N. H. Damrauer, G. Cerullo, A. Yeh, T. R. Boussie, C. V Shank and J. K. McCusker, *Science*, 1997, **275**, 54–57.

7 A. El Nahhas, A. Cannizzo, F. van Mourik, A. M. Blanco-Rodríguez, S. Zális, A. Vlcek and M. Chergui, *J. Phys. Chem. A*, 2010, **114**, 6361–6369.

8 S. E. Canton, K. S. Kjær, G. Vankó, T. B. van Driel, S. Adachi, A. Bordage, C. Bressler, P. Chabera, M. Christensen, A. O. Dohn, A. Galler, W. Gawelda, D. Gosztola, K. Haldrup, T. Harlang, Y. Liu, K. B. Møller, Z. Németh, S. Nozawa, M. Pápai, T. Sato, T. Sato, K. Suarez-Alcantara, T. Togashi, K. Tono, J. Uhlig, D. A. Vithanage, K. Wärnmark, M. Yabashi, J. Zhang, V. Sundström and M. M. Nielsen, *Nat. Commun.*, 2015, **6**, 6359.

9 P. F. Barbara, T. J. Meyer and M. A. Ratner, *J. Phys. Chem.*, 1996, **100**, 13148–13168.

10 M. Galperin, M. a Ratner, A. Nitzan and A. Troisi, *Science*, 2008, **319**, 1056–1060.

11 J. Sukegawa, C. Schubert, X. Zhu, H. Tsuji, D. M. Guldi and E. Nakamura, *Nat. Chem.*, 2014, **6**, 899–905.

12 C. Schnedermann, M. Liebel and P. Kukura, *J. Am. Chem. Soc.*, 2015, **137**, 2886–2891.

13 J. N. Schrauben, K. L. Dillman, W. F. Beck and J. K. McCusker, *Chem. Sci.*, 2010, **1**, 405–410.

14 Y. Yue, T. Grusenmeyer, Z. Ma, P. Zhang, R. H. Schmehl, D. N. Beratan and I. V Rubtsov, *Dalt. Trans.*, 2015, **44**, 8609–8616.

15 Y. Yue, L. N. Qasim, A. A. Kurnosov, N. I. Rubtsova, R. T. Mackin, H. Zhang, B. Zhang, X. Zhou, J. Jayawickramarajah, A. L. Burin and I. V Rubtsov, *J. Phys. Chem. B*, 2015, 6448–6456.

16 A. Harriman, M. Hissler, O. Trompette, R. Ziessel and L. Pasteur, 1999, 2516–2525.

17 J. E. Yarnell, J. C. Deaton, C. E. McCusker and F. N. Castellano, *Inorg. Chem.*, 2011, **50**, 7820–7830.

18 D. J. Stufkens and A. Vlcek, 1998, **177**, 127–179.

19 A. Cannizzo, A. M. Blanco-Rodríguez, A. El Nahhas, J. Sebera, S. Zális, A. Vlcek and M. Chergui, *J. Am. Chem. Soc.*, 2008, **130**, 8967–8974.

20 M. E. Walther, J. Grilj, D. Hanss, E. Vauthey and O. S. Wenger, *Eur. J. Inorg. Chem.*, 2010, **2010**, 4843–4850.

21 L. M. Kiefer, J. T. King and K. J. Kubarych, *Acc. Chem. Res.*, 2015, **48**, 1123–1130.

22 A. El Nahhas, C. Consani, A. M. Blanco-Rodríguez, K. M. Lancaster, O. Braem, A. Cannizzo, M. Towrie, I. P. Clark, S. Zális, M. Chergui and A. Vlcek, *Inorg. Chem.*, 2011, **50**, 2932–2943.

23 P. Paoprasert, J. E. Laaser, W. Xiong, R. A. Franking, R. J. Hamers, M. T. Zanni, J. R. Schmidt and P. Gopalan, *J. Phys. Chem. C*, 2010, **114**, 9898–9907.

24 M. Hissler, W. B. Connick, D. K. Geiger, J. E. McGarrah, D. Lipa, R. J. Lachicotte and R. Eisenberg, *Inorg. Chem.*, 2000, **39**, 447–457.

25 J. E. McGarrah and R. Eisenberg, *Inorg. Chem.*, 2003, **42**, 4355–4365.

26 S. Archer and J. A. Weinstein, *Coord. Chem. Rev.*, 2012, **256**, 2530–2561.

27 E. A. Glik, S. Kinayyigit, K. L. Ronayne, M. Towrie, I. V Sazanovich, J. A. Weinstein and F. N. Castellano, *Inorg. Chem.*, 2008, **47**, 6974–6983.

28 E. O. Danilov, I. E. Pomestchenko, S. Kinayyigit, P. L. Gentili, M. Hissler, R. Ziessel and F. N. Castellano, *J. Phys. Chem. A*, 2005, **109**, 2465–2471.

29 E. O. Danilov, A. A Rachford, S. Goeb and F. N. Castellano, *J. Phys. Chem. A*, 2009, **113**, 5763–5768.

30 H. Guo, M. L. Muro-Small, S. Ji, J. Zhao and F. N. Castellano, *Inorg. Chem.*, 2010, **49**, 6802–6804.

31 M. L. Muro, A. A. Rachford, X. Wang and F. N. Castellano, *Top Organomet Chem*, 2010, **29**, 159–191.

32 E. C.-H. Kwok, M.-Y. Chan, K. M.-C. Wong and V. W.-W. Yam, *Chem Eur J*, 2014, **20**, 3142–3153.

33 C.-H. Tao, N. Zhu and V. W.-W. Yam, *Chem Eur J*, 2005, **11**, 1647–1657.

34 K. Kim, S. Liu, M. E. Kose and K. S. Schanze, *Inorg. Chem.*, 2006, **45**, 2509–2519.

35 C. E. Whittle, J. A. Weinstein, M. W. George and K. S. Schanze, *Inorg. Chem.*, 2001, **40**, 4053–4062.

36 J. M. Keller, K. D. Glusac, E. O. Danilov, S. McIlroy, P. Sreearuothai, A. R. Cook, H. Jiang, J. R. Miller and K. S. Schanze, *J. Am. Chem. Soc.*, 2011, **133**, 11289–11298.

37 R. Sugimura, S. Suzuki, M. Kozaki, K. Keyaki, K. Nozaki, H. Matsushita, N. Ikeda and K. Okada, *Res. Chem. Intermed.*, 2013, **39**, 185–204.

38 M. Delor, P. A. Scattergood, I. V Sazanovich, A. W. Parker, G. M. Greetham, A. J. H. M. Meijer, M. Towrie and J. A. Weinstein, *Science*, 2014, **346**, 1492–1495.

39 P. A. Scattergood, M. Delor, I. V Sazanovich, O. V Bouganov, S. A. Tikhomirov, A. S. Stasheuski, A. W. Parker, G. M. Greetham, M. Towrie, E. S. Davies, A. J. H. M. Meijer and J. A. Weinstein, *Dalt. Trans.*, 2014, **43**, 17677–17693.

40 G. Zhou, W.-Y. Wong, S.-Y. Poon, C. Ye and Z. Lin, *Adv. Funct. Mater.*, 2009, **19**, 531–544.

41 L. Liu, D. Huang, S. M. Draper, X. Yi, W. Wu and J. Zhao, *Dalt. Trans.*, 2013, **42**, 10694–10706.

42 C. Liao, J. E. Yarnell, K. D. Glusac and K. S. Schanze, *J. Phys. Chem. B*, 2010, **114**, 14763–14771.

43 R. Packheiser, P. Ecorchard, T. Ru and H. Lang, *Organometallics*, 2008, **27**, 3534–3546.

44 F. Nolde, J. Qu, C. Kohl, N. G. Pschirer, E. Reuther and K. Müllen, *Chem. - A Eur. J.*, 2005, **11**, 3959–3967.

45 P. D. Frischmann, K. Mahata and F. Würthner, *Chem. Soc. Rev.*, 2013, 1847–1870.

46 D. Gosztola, M. P. Niemczyk, W. Svec, A. S. Lukas and M. R. Wasielewski, *J. Phys. Chem. A*, 2000, **104**, 6545–6551.

47 H. Langhals, R. Ismael and O. Yürük, *Tetrahedron*, 2000, 56, 5435–5441.

48 F. N. Castellano, *Dalton Trans.*, 2012, **41**, 8493–8501.

49 I. V Sazanovich, M. A. H. Alamiry, A. J. H. M. Meijer, M. Towrie, E. S. Davies, R. D. Bennett and J. A. Weinstein, *Pure Appl. Chem.*, 2013, **85**, 1331–1348.

50 I. V Sazanovich, M. A. H. Alamiry, J. Best, R. D. Bennett, O. V Bouganov, E. S. Davies, V. P. Grivin, A. J. H. M. Meijer, V. F. Plyusnin, K. L. Ronayne, A. H. Shelton, S. A. Tikhomirov, M. Towrie and J. A. Weinstein, *Inorg. Chem.*, 2008, **47**, 10432–10445.

51 J. M. Keller and K. S. Schanze, *Organometallics*, 2009, **28**, 4210–4216.

52 D. Hanss and O. S. Wenger, *Eur. J. Inorg. Chem.*, 2009, **2009**, 3778–3790.

53 T. C. Barros, S. Brochsztain, V. G. Toscano, P. B. Filho and M. J. Politi, *J. Photochem. Photobiol. A Chem.*, 1997, 111, 97–104.

54 S. R. Greenfield, W. A. Svec, D. Gosztola and M. R. Wasielewski, *J. Am. Chem. Soc.*, 1996, **118**, 6767–6777.

55 J. E. Rogers and L. A. Kelly, *J. Am. Chem. Soc.*, 1999, **121**, 3854–3861.

56 N. M. Shavaleev, E. S. Davies, H. Adams, J. Best and J. A. Weinstein, *Inorg. Chem.*, 2008, **47**, 1532–1547.

57 N. M. Shavaleev, H. Adams, J. Best and J. A. Weinstein, *J. Organomet. Chem.*, 2007, **692**, 921–925.

58 M. Hissler, J. E. McGarrah, W. B. Connick, D. K. Geiger, S. D. Cummings and R. Eisenberg, *Coord. Chem. Rev.*, 2000, **208**, 115–137.

59 I. V Sazanovich, J. Best, P. a. Scattergood, M. Towrie, S. a. Tikhomirov, O. V Bouganov, A. J. H. M. Meijer and J. a. Weinstein, *Phys. Chem. Chem. Phys.*, 2014, **16**, 25775–25788.

60 M. Delor, T. Keane, P. A. Scattergood, I. V Sazanovich, G. M. Greetham, M. Towrie, A. J. H. M. Meijer and J. A. Weinstein, *Nat. Chem.*, 2015, **accepted**.

61 M. Delor, I. V Sazanovich, M. Towrie and J. A. Weinstein, *Acc. Chem. Res.*, 2015.

62 G. M. Greetham, P. Burgos, Q. Cao, I. P. Clark, P. S. Codd, R. C. Farrow, M. George, M. Kogimtzis, P. Matousek, A. W. Parker, M. R. Pollard, D. A. Robinson, Z.-J. Xin and M. Towrie, *Appl. Spectrosc.*, 2010, **64**, 1311–1319.

63 J. J. Snellenburg, S. P. Laptenok, R. Seger, K. M. Mullen and I. H. M. van Stokkum, *J. Stat. Softw.*, 2012, **49**, 1–22.